Microsc. Microanal. 16, 210–217, 2010
doi:10.1017/S1431927609991371

Microscopy AND Microanalysis

© MICROSCOPY SOCIETY OF AMERICA 2010

# Three-Dimensional Analysis of Carbon Nanotube Networks in Interconnects by Electron Tomography without Missing Wedge Artifacts

Xiaoxing Ke,[1,*] Sara Bals,[1] Daire Cott,[2] Thomas Hantschel,[2] Hugo Bender,[2] and Gustaaf Van Tendeloo[1]

[1]*EMAT, University of Antwerp, Groenenborgerlaan 171, B-2020 Antwerp, Belgium*
[2]*IMEC, Kapeldreef 75, B-3001 Leuven, Belgium*

**Abstract:** The three-dimensional (3D) distribution of carbon nanotubes (CNTs) grown inside semiconductor contact holes is studied by electron tomography. The use of a specialized tomography holder results in an angular tilt range of ±90°, which means that the so-called "missing wedge" is absent. The transmission electron microscopy (TEM) sample for this purpose consists of a micropillar that is prepared by a dedicated procedure using the focused ion beam (FIB) but keeping the CNTs intact. The 3D results are combined with energy dispersive X-ray spectroscopy (EDS) to study the relation between the CNTs and the catalyst particles used during their growth. The reconstruction, based on the full range of tilt angles, is compared with a reconstruction where a missing wedge is present. This clearly illustates that the missing wedge will lead to an unreliable interpretation and will limit quantitative studies.

**Key words:** electron tomography, carbon nanotubes, missing wedge, FIB, TEM, patterned nanostructures

## Introduction

Sizes in integrated circuits (IC) have now reached the nanometer range and the use of copper as an interconnect material has met its lower size limit (Steinlesberger et al., 2002; Li et al., 2003; Ingerly et al., 2008). Carbon nanotubes (CNTs) are considered as an ideal alternative because of their unique properties, particularly their high thermal conductivity, low resistance, and ballistic transport, etc. (Kreupl et al., 2002; Li et al., 2003; Nihei et al., 2003; Srivastava et al., 2005; Li et al., 2007). Recently, the growth of CNTs has been demonstrated in so-called "contact holes" using a variety of catalyst particles to simulate on-chip contact-hole interconnects (Nihei et al., 2003, 2005; Sato et al., 2006; Hantschel et al., 2008; Zhang et al., 2008). However, more effort is required to characterize these structures on a local scale, including the interface between the CNTs and the contact hole or catalyst. Based on such information, the growth of the CNTs including the function of the catalyst material can be better understood and optimized.

A powerful method to investigate such samples is transmission electron microscopy (TEM). Sample preparation for this purpose is unfortunately not straightforward and one should use a site-specific technique while preserving the CNT structure. A previous TEM study succeeded in showing the two-dimensional (2D) nanostructure of a single CNT grown in a contact hole (Ke et al., 2009). However, contact holes containing a higher density of CNTs are of more importance as the resistance can be lowered by increasing the density to outperform and eventually replace Cu interconnects (Nihei et al., 2003; Srivastava et al., 2005; Li et al., 2007). This complicates the CNT analysis by conventional 2D TEM due to overlapping of three-dimensional (3D) networks in 2D projections. Therefore, it is necessary to investigate these structures using electron tomography.

Electron tomography basically consists of three steps: acquisition of a tilt series of 2D projections, alignment of the projections, and 3D reconstruction. Although the TEM acquisition techniques may vary to obtain tilt series featuring structural information or chemical details (Möbus & Inkson, 2001; Midgley & Weyland, 2003; Möbus et al., 2003; Bals et al., 2006, 2007; Gass et al., 2006; Kolb et al., 2007), the angular tilt range over which the 2D projections can be acquired is mostly limited. This is due to the limited space for the specimen holder between the objective lens pole pieces. Even a dedicated tomography holder typically has a tilting range of only ±80°. As a consequence, so-called "missing wedge" artifacts can be expected in the 3D reconstructions (Midgley & Weyland, 2003). These artifacts will hamper qualitative and quantitative interpretation of the

Received August 21, 2009; accepted December 22, 2009
**Corresponding author*. E-mail: Xiaoxing.Ke@ua.ac.be

3D reconstructed volume. Solutions such as "discrete tomography" have been proposed to solve this problem (Bals et al., 2007; Bals et al., 2009; Batenburg et al., 2009; Turner et al., 2009). Here, we have used a 360° on-axis rotation tomography holder that is able of acquiring a full tilt series without missing wedge. This type of holder was recently used to study a variety of samples such as a zirconia/polymer nanocomposite sample and a semiconductor device (Kawase et al., 2007; Yaguchi et al., 2008; Jarausch et al., 2009). In all these studies, dedicated samples were prepared by focused ion beam (FIB) milling. Indeed, for tilting at high angles, the effective specimen thickness steeply increases and hence dedicated sample preparation in the form of pillars is required. Moreover, in this study, sample preparation needs to be site specific because the aim is to capture a complete contact hole, but in addition the use of FIB milling should be carried out using a dedicated procedure because the CNTs should remain intact after the sample preparation.

After acquisition and reconstruction of the tilt series, the 3D reconstructed volume is segmented and visualized. The CNT network is revealed and therefore its distribution in the contact hole is estimated in a quantitative manner. The 3D results are combined with high-resolution transmission electron microscopy (HRTEM) and analytical results obtained using energy dispersive X-ray spectroscopy (EDX) to investigate the relation between the CNT network and the catalyst particles.

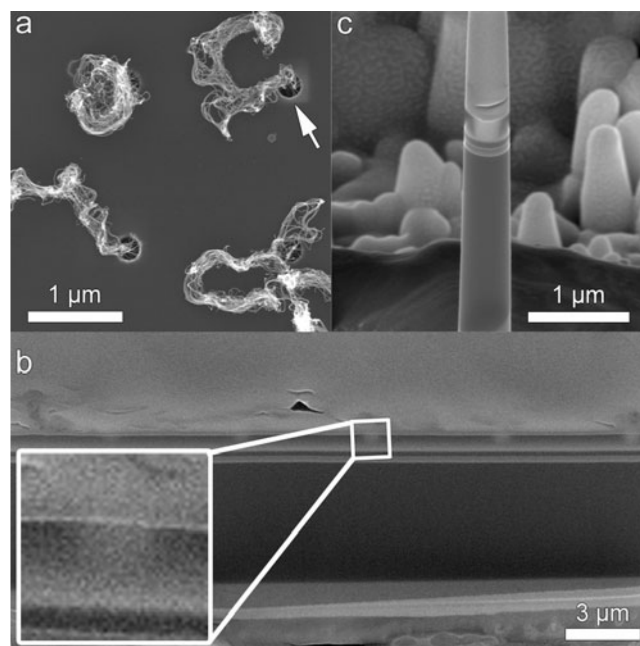


**Figure 1.** **a:** SEM image of the specimen's surface shows arrays of contact holes with CNTs growing out. The contact holes are half-open because they are not fully covered by bundles of CNTs, as indicated by arrow. **b:** The contrast of contact holes appears when the edge of the lamella is approaching their sidewalls by FIB milling. The magnified inset shows such an example. The white contrast defines the contact holes embedded in the dark contrast of $SiO_2$ matrix. **c:** The FIB-prepared micropillar sample containing the entire contact hole.

## Materials and Methods

### Materials

The sample consists of a 100 nm thermal $SiO_2$ layer on a silicon substrate. On top of the $SiO_2$ a 15/10 nm layer of Ti/TiN was deposited for adhesion and to prevent W diffusion, respectively. The bottom contact layer consisted of 70 nm W with a 30 nm SiC used as an etch stop layer. On top, an amorphous 300 nm $SiO_2$ layer was deposited in which the contact holes were etched. The diameter of the contact holes ranged from 130 to 300 nm. A 1 nm nominal thickness Fe film was sputtered onto the surface, coating the contact holes as well. The Fe film was annealed into catalytic nanoparticles using an $H_2$ plasma (Romo-Negreira et al., 2008). To remove the catalyst nanoparticles from the top $SiO_2$ surface, a sacrificial spin-on polymer was deposited that filled the contact holes to protect the confined catalyst during removal by chemical mechanical polishing (Esconjaureguil et al., 2008). Multiwalled CNTs (MWCNTs) were grown inside the contact holes by chemical vapor deposition using an Oxford Instruments NANO PECVD reactor (Romo-Negreira et al., 2008). Bundles of MWCNTs grow inside and out of the contact holes, as illustrated by scanning electron microscopy (SEM) image in Figure 1a. Here, the 250 nm contact holes are investigated.

### FIB Sample Preparation

A micropillar is prepared using site-specific FIB milling (Kawase et al., 2007; Yaguchi et al., 2008; Jarausch et al., 2009) to be mounted onto the Fischione model 2050 on-axis rotation tomography holder. FIB sample preparation is performed using a FEI Nova 200 Nanolab DualBeam SEM/FIB system. The system is equipped with an *in situ* gas injection system loaded with a Pt deposition needle and an OMNIPROBE™ extraction needle.

Prior to milling, a dual cap protective Pt layer is applied: an electron beam induced Pt deposition (EBID) of approximately 600 nm is followed by ion beam induced Pt deposition (IBID) of approximately 1.5 $\mu$m (Thompson et al., 2007; Ke et al., 2009). The use of EBID Pt prior to IBID Pt is essential to protect the CNTs because the IBID damage has a typical depth of damage of 100–200 nm due to the energetic $Ga+$ ions used during deposition (Montoya, 2007). It has been shown that EBID deposition can dramatically reduce the amorphization damage depth by using the low energy electron beam (Montoya et al., 2007). On this specimen, the Pt layer is approximately 2.5 $\mu$m wide $\times$ 10 $\mu$m long, covering a short array of contact holes.

Next, a lamella is prepared using the normal lift-out procedure (Giannuzzi & Stevie, 2005; Montoya et al., 2007;

Ke et al., 2009) and is welded to a specimen post that can be mounted on the 360° on-axis rotation tomography holder. In the following step, the specimen is gradually thinned using a 30 kV ion beam and a current of 0.1 nA. Since the specimen contains contact holes approximately in the middle of the lamella, a different contrast is obtained in the SEM image, when the edges of the lamella approach the contact holes during milling. With an 18 kV SEM beam, this contrast appears approximately 200 nm away from the contact hole. Once such contrast is observed as shown in Figure 1b, the stage is rotated over 180° and the same thinning procedure is repeated at the other side of the specimen. By then the lamella has a thickness of about 650 nm. To select one contact hole from the array of contact holes present in the lamella, the same thinning procedure is repeated at the left and right side of the selected contact hole. Due to the fact that the effective specimen thickness steeply increases for high tilt angles, a pillar sample is required to cover a tilt range of ±90°. Therefore, in a next step, a micropillar with uniform thickness is obtained using a circle/ring patterning together with an ion beam of 30 kV energy and 30 pA current. The inner diameter of the ring pattern is set to decrease gradually from 800 nm to 600 nm. As the 30 kV ion beam leaves a thick damaged amorphous layer on the specimen side walls due to the high beam energy, low kV thinning is necessary to reduce the amorphous damage while further thinning the specimen. A 10 kV ion beam with a current of 16 pA is applied for the final thinning and cleaning. In this manner, the inner diameter of the ring pattern is reduced to 450 nm. Note that in the present case this damage does not really cause a problem; the oxide is anyhow amorphous and the amorphization at the pillar edges in the Si is not considered. Thinning is closely monitored by SEM from different perspectives to verify that the complete contact hole remains included inside the micropillar. The final as-prepared specimen is shown in Figure 1c.

### Electron Tomography and TEM Investigation

A high-angle annular dark-field scanning transmission electron microscopy (HAADF-STEM) tilt series of the FIB prepared micropillar is acquired on a JEOL3000F microscope using the Fischione model 2050 on-axis rotation tomography holder. During the acquisition of the HAADF-STEM tilt series, the inner detector angle is set to be 60 mrad; a nominal 0.2 nm STEM probe is applied; acquisition time of one image is about 40.9 s. The acquired images have a pixel size of 1.5 nm. The tilt series has an angular range of ±90° with projections taken every 2°, which is considered as a compromise between a good-quality reconstruction and the minimization of radiation artifacts during acquisition. Alignment of the tilt series is done using the FEI Inspect3D software. The same software is used to reconstruct the aligned tilt series through the Simultaneous Iterative Reconstruction Technique (SIRT) (Gilbert, 1972). The volume reconstructed by SIRT is segmented manually and visualized in the Amira software.

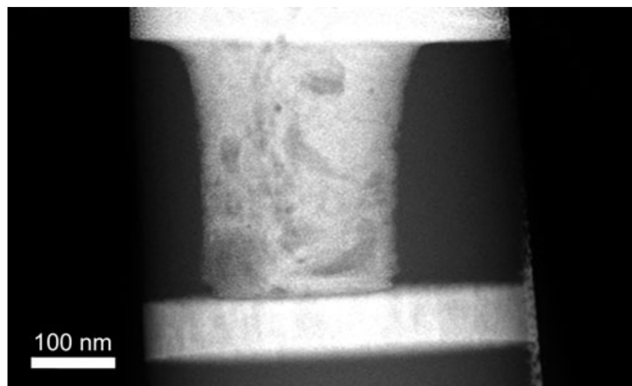


**Figure 2.** HAADF-STEM image from the acquired tilt series showing the contact hole. The white intensity reveals that the contact hole is filled with Pt as a result of the Pt protective layer deposition. CNTs cannot be observed in a straightforward manner from a single 2D projection.

HRTEM and EDX in scanning mode (STEM-EDX) are carried out on the JEOL 3000F microscope, using lamella-shaped samples prepared by FIB as explained in Ke et al. (2009).

## Results

### 3D Distribution of the CNTs

A 2D HAADF-STEM image from the tilt series is presented in Figure 2. From this image, the diameter of the micropillar specimen is determined to be 470 nm. The contact hole can be clearly distinguished, and the diameter is measured to be approximately 250 nm. It can be seen that Pt, which was used as a protection layer during the FIB preparation process, has partially filled the contact hole because the contact hole is not completely covered by CNTs (Fig. 1a). Since the intensity, present in a HAADF-STEM image, approximately scales with the square of the atomic number Z, the Pt-filled contact hole shows a much brighter intensity than the surrounding amorphous $SiO_2$. For the same reason, the large contrast difference between Pt and C helps to distinguish the CNT networks from the Pt-filling inside the contact holes (see Fig. 2), although the CNTs cannot be directly revealed in a single 2D projection image because of overlapping of the 3D volume.

Orthogonal slices through the 3D reconstructed volume based on the SIRT algorithm are presented in Figure 3. As shown in Figure 3a, a cross section from the reconstruction of the micropillar proves that the entire contact hole is included inside the micropillar, which means that the contact hole is kept intact. Figure 3b–d present three orthogonal slices through the reconstruction of the contact hole.

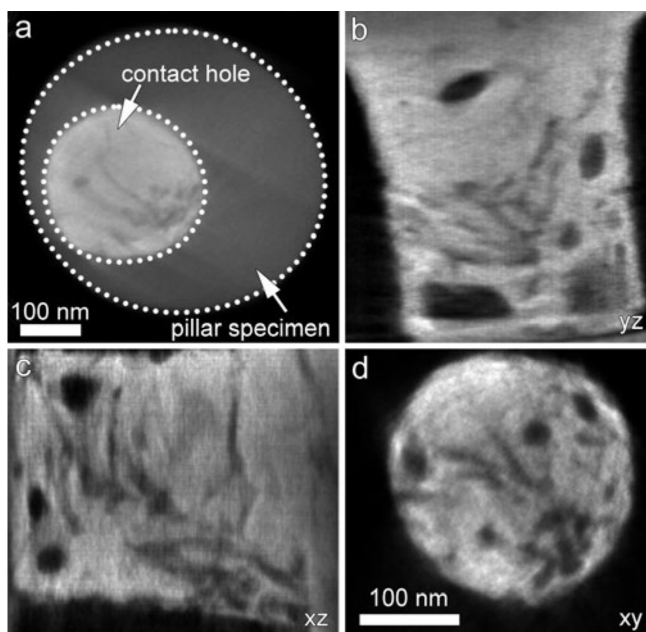


**Figure 3.** Orthogonal slices of the reconstruction by SIRT. **a:** An orthogonal slice through the pillar shape specimen showing that the entire contact hole is kept intact. **b–d:** Three orthogonal slices through the contact hole.

The presence of holes in the Pt material can be clearly observed, indicating that the contact hole is not completely filled with Pt. More important is that CNTs are clearly visible in these orthogonal slices, which means that they were preserved during the TEM specimen preparation. The cross sections of the micropillar and the contact hole both appear circular in Figure 3a,d. It is therefore clear that missing wedge artifacts have been avoided because they usually appear as an elongation of the structure and would lead to deviations from circular structures (Midgley & Weyland, 2003; Bals et al., 2007).

To obtain a 3D visualization, the 3D reconstruction is manually segmented and the result is presented in Figure 4 and in a movie, which can be found as supplementary file.

**Supplementary Movie**

A supplementary movie is available online (please visit journal.cambridge.org/jid_MAM).

The CNTs can be distinguished by their obvious difference in morphology and the difference in the intensity of the pixels as measured in orthoslices through the final 3D reconstruction. The network of the CNTs inside the contact

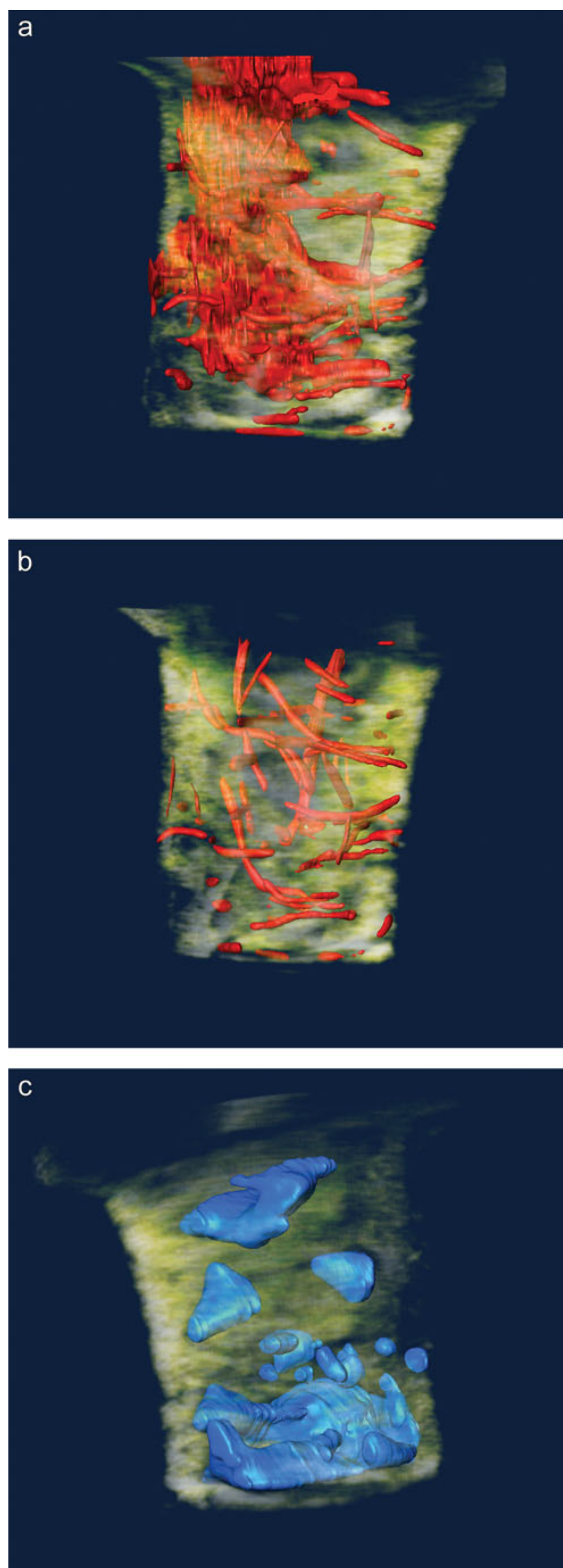


**Figure 4.** Snapshots of the contact hole's reconstruction in 3D prospect, showing (**a**) the network of all CNTs, (**b**) the network of isolated CNTs, and (**c**) voids distribution inside the contact hole.

hole is shown in Figure 4a. Note that in this particular sample the CNTs are distributed randomly rather than in a preferred vertical orientation. Furthermore, the majority of the CNTs is attached to the inner wall of the contact hole. In the lower part of the contact hole, individual CNTs or small bundles of CNTs are scattered. However, most of the CNTs are found to be bundled and tangled in the upper part, close to the opening of the contact hole. A network of isolated CNTs can be recognized from the reconstructed slices, as shown in Figure 4b. Voids in the Pt material inside the contact holes are illustrated in Figure 4c.

When studying the use of CNTs as innerconnects, quantitative measurements concerning the CNTs network are important. The filling density of the CNTs inside the contact hole and the average CNT diameter are important parameters, which can be computed in a straightforward way from the 3D reconstruction. By dividing the volume of the CNTs with that of the contact hole, the filling density is found to be approximately 14%. Estimating the diameter of the CNTs, however, is still not straightforward because the majority of the CNTs appear bundled. Therefore, only the diameters of the isolated CNTs (Fig. 4b) are used to determine an average diameter that was found to equal 8.2 nm ±0.3 nm, in good agreement with similar synthesis conditions (Romo-Negreira et al., 2008). It must be noted that the error of 0.3 nm here is the standard deviation on the mean and may not be confused with the standard deviation on an individual measurement, which should ultimately be set by the pixel size. The volume ratio of isolated CNTs to bundled CNTs is computed to be approximately 22%.

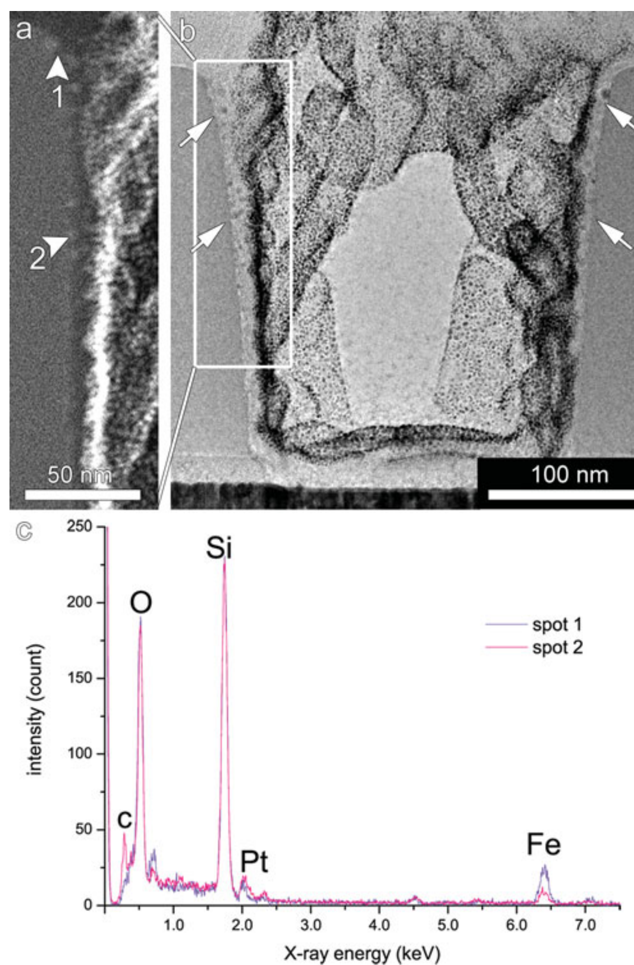


**Figure 5.** A (S)TEM study of the contact hole reveals the distribution of Fe catalyst particles. **a:** A part of the HAADF-STEM image of the contact hole that is shown completely in TEM image **b**. As indicated by arrows in panel **b**, particles are found to be scattered along the side wall of the contact hole. The particles are seen in panel **a** as well with light gray contrast. EDX point analysis is carried out at positions indicated by circles in panel **a**. The spectra are presented in panel **c** that both show Fe intensities.

## Catalyst Material

To study the relation between the Fe catalyst material and the growth of the CNTs, the presence of the catalyst material was investigated by STEM-EDX. Since the micropillar is too thick to obtain HRTEM images and reliable EDX signals simultaneously, a thin lamella sample was prepared by FIB through the middle of another contact hole from the same specimen. STEM-EDX spot analysis reveals no Fe signals when probing the middle of the contact hole, but when probing the side walls of the contact hole, the EDX spectra show significant intensities of Fe (Fig. 5). A high magnification HAADF-STEM image of the contact hole is shown in Figure 5a together with the corresponding HRTEM image in Figure 5b. The majority of the contact hole is decorated with particles. These particles are Pt nanocrystals from the Pt protective layers. These Pt nanocrystals usually have extremely uniform size distribution and have higher contrast due to their high Z number. Nevertheless, along the side walls of the contact hole, particles with different contrast and slightly larger sizes are present (indicated by arrows in Fig. 5b). The EDX spectra taken in the corresponding areas indicated as 1 and 2 in Figure 5a are shown in Figure 5c and Fe intensities are clearly present. From the HAADF-STEM and HRTEM images, it is found that the majority of these particles are attached to the upper part of the side walls of the contact hole, whereas fewer particles are found in the lower areas of the contact hole. This is also confirmed by EDX measurements, as the Fe intensity from the upper side walls was found to be higher in comparison to lower areas.

It must be noted that the catalyst particles cannot be observed in the 3D reconstruction because of the small sizes. From HRTEM images, the diameters of the catalyst particles are measured to be approximately 2 nm and in the HAADF-STEM tilt series each pixel equals 1.5 nm, which means the catalyst particles are represented by no more than two pixels. Although the Pt nanocrystals also have even smaller sizes as revealed by HRTEM, they cover a large area

with high density in the contact hole and therefore can be reconstructed as a continuous volume.

## Discussion

Using electron tomography the distribution of CNTs in a contact hole has been investigated. It was found that in the present sample, the CNTs are preferably attached to the walls of the contact holes with a higher density of CNT present near the top of the contact hole. We believe that the origin of this sidewall growth can be attributed in part to the catalyst deposition technique as the Fe sputtering was nonselective to the bottom of the via and a considerable portion of the side walls were exposed to deposition. To avoid this negative sidewall CNT growth such techniques as selective electrochemical catalyst deposition (Romo-Negreira et al., 2009), laser ablation and size selective oriented deposition (Sato et al., 2006) have been demonstrated. Nevertheless, to understand the CNT growth behavior in this particular via and the correlation with the presence of the catalyst particles used during growth of the CNTs, the distribution of the catalyst particles was investigated by STEM-EDX in combination with HAADF-STEM and HRTEM. It was found that the Fe particles are indeed present at the side walls of the contact holes with a higher density near the top of the contact hole as well. This explains the fact that many of the CNTs have their one ends attached to the side walls of the contact hole. Moreover, the particles' higher density at the upper part of the contact hole may lead to the bundling of multiple CNTs near the top of the contact hole. Similarly, only few CNTs are found near the bottom of the contact hole primarily due to the fact that only few catalyst particles are present in that area. Additionally, the difference in the underlying material supporting the metal catalyst ($SiO_2$, sidewall; W, contact layer in the bottom of the contact hole) should also be considered. In previous work we have observed a lower CNT density when grown directly on W compared to the more conventionally used silicon oxide support. Furthermore, it is unlikely that the CNTs grown from the top portion of the contact hole will inhibit the gas precursor transport to the bottom of the contact hole as estimated from the CNT filling density of 14%. Notwithstanding, in this particular sample, CNT growth from the contact hole highlighted the importance of having a tight control over both the location and density of the metal catalyst when integrating CNTs in patterned Si structures.

### Avoiding the Missing Wedge

Using a dedicated tomography holder and a micropillar TEM sample, 3D results have been obtained without the missing wedge. In Figure 6, the effect of the missing wedge is investigated by comparing the reconstruction based on the full 180° tilt range to one using a 140° tilt range

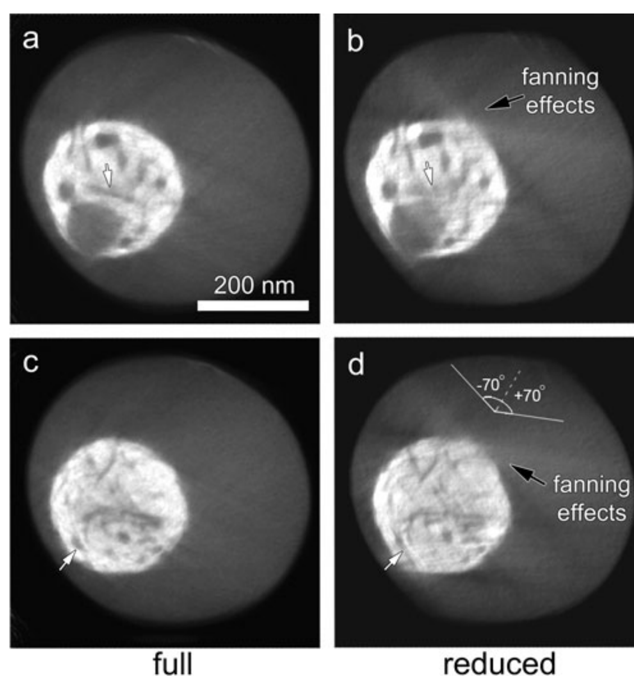


**Figure 6.** Slices taken at two different positions through the 3D reconstruction based on (**a,c**) a tilt series with full rotation ±90° and (**b,d**) a series with reduced angles ±70°. **b,d:** Fanning effects due to the missing wedge are indicated by black arrows. **a:** A CNT is clearly observed (white arrow) but is smeared out by artifacts in the slice shown in panel **b** that was taken at the same position. **d:** A fanning effect indicated by a white arrow might be misinterpreted as a CNT.

(−70°/+70°); this was done using the same dataset but neglecting the images taken at higher angles. In the latter case, a clear elongation and fanning artifacts typical for a missing wedge are present. For a quantitative interpretation, it is very important that the segmentation step in the tomography process is carried out in a reliable manner. This segmentation step is required to determine the correspondence between different grayscales in the reconstruction and different compositions in the original structure. This segmentation step is often time consuming and, even more important, subjective. As shown in Figure 6b, fanning artifacts smear out a CNT that is clearly present in Figure 6a; in Figure 6d, a fanning artifact may be interpreted as the presence of a CNT that is in fact a hole in Figure 6c. Obviously, such artifacts will lead to a wrong quantification of the reconstruction, and it is therefore extremely important to overcome the missing wedge problem. Since the missing wedge is eliminated in a ±90° experiment, the use of a 360° rotation tomography holder is often regarded as the ultimate manner to obtain quantitative results in 3D. However, other minor reconstruction artifacts such as the effect of a limited sampling and slight misalignments might still be present (Midgley & Weyland, 2003). In Figure 6, it has been illustrated that even when missing wedge artifacts are avoided, it is still difficult to define the boundaries of

the CNTs. This makes it very clear that segmentation is not always straightforward. Discrete tomography is a very promising technique toward automatic segmentation as proposed in recent studies (Bals et al., 2007, 2009; Batenburg et al., 2009), because the segmentation step is performed *in situ* during the reconstruction. At present, manual segmentation is still unavoidable. Although it may not lead to *absolute* certainty in quantification, it has been successfully shown that avoiding missing wedge artifacts is an important step toward quantitative information in 3D.

## Conclusions

The main goal of this research was to develop and optimize a 3D electron tomography approach for supporting the CNT process development. The specimen is prepared by a dedicated FIB procedure, leaving the contact hole as well as the CNTs intact. Three-dimensional reconstructions based on a conventional SIRT algorithm show that the CNTs originate from the side walls of the contact hole with a higher CNT density near the top of the contact hole. This can be understood because HRTEM and STEM-EDX showed that the catalyst particles are present at the side walls of the contact holes as well. Note that this side wall growth is induced by the use of sputtered Fe as catalyst material and should be avoided for real applications. Finally, it has been discussed that missing-wedge-free electron tomography is very powerful; the use of on-axis rotation holder implements the acquisition of the tilt series covering 360° and therefore results in a missing wedge free reconstruction. The minimization of the fanning and elongation effects greatly reduces the misinterpretation of the CNTs, which leads to a relatively reliable quantitative result of the 3D reconstruction.

## Acknowledgments

The authors acknowledge financial support from the European Union under the Framework 6 program under a contract for an Integrated Infrastructure Initiative, Reference 026019 ESTEEM. S.B. is grateful to the Fund for Scientific Research-Flanders. Part of this work was supported by the FWO project G.0180.08. This work was partly supported by the IAP-VI framework of the Belgian government and by the EU project CARBonCHIP (NMP4-CT-2006-016475). Sywert Brongersma is acknowledged for Fe deposition at IMEC NL Holst Centre, H.T.C. Eindhoven, The Netherlands.

## References

Bals, S., Batenburg, K.J., Liang, D., Lebedev, O., Van Tendeloo, G., Aerts, A., Martens, J.A. & Kirschhock, C.E.A. (2009). Quantitative three-dimensional modeling of zeotile through discrete electron tomography. *J Am Chem Soc* **131**, 4769–4773.

Bals, S., Batenburg, K.J., Verbeeck, J., Sijbers, J. & Van Tendeloo, G. (2007). Quantitative three-dimensional reconstruction of catalyst particles for bamboo-like carbon nanotubes. *Nano Lett* **7**, 3669–3674.

Bals, S., Van Tendeloo, G. & Kisielowski, C. (2006). A new approach for electron tomography: Annular dark-field transmission electron microscopy. *Adv Mater* **18**, 892–895.

Batenburg, K.J., Bals, S., Sijbers, J., Kübel, C., Midgley, P.A., Hernandez, J.C., Kaiser, U., Encina, E.R., Coronado, E.A. & Van Tendeloo, G. (2009). 3D imaging of nanomaterials by discrete tomography. *Ultramicroscopy* **109**, 730–734.

Esconjaureguil, S., Whelan, C.M. & Maex, K. (2008). Patterning of metallic nanoparticles for the growth of carbon nanotubes. *Nanotechnology* **19**, 135306. Available at http://www.iop.org/EJ/abstract/0957-4484/19/13/135306/.

Gass, M.H., Koziol, K.K.K., Windle, A.H. & Midgley, P.A. (2006). Four-dimensional spectral tomography of carbonaceous nanocomposites. *Nano Lett* **6**, 376–379.

Giannuzzi, L.A. & Stevie, F.A. (2005). *Introduction to Focused Ion Beams*. New York: Springer.

Gilbert, P. (1972). Iterative methods for 3-dimensional reconstruction of an object from projections. *J Theor Biol* **36**, 105–117.

Hantschel, T., Ryan, P., Palanne, S., Richard, O., Arstila, K., Verhulst, A.S., Bender, H., Ke, X. & Vandervorst, W. (2008). Nanoprober-based pick-and-place process for site-specific characterization of individual carbon nanotubes. In *Materials Research Society Symposium Proceedings*, pp. 1081-P17-04. San Francisco, CA: Materials Research Society.

Ingerly, D., Agraharam, S., Becher, D., Chikarmane, V., Fischer, K., Grover, R., Goodner, M., Haight, S., He, J., Ibrahim, T., Joshi, S., Kothari, H., Lee, K., Lin, Y., Litteken, C., Liu, H., Mays, E., Moon, P., Mule, T., Nolen, S., Patel, N., Pradhan, S., Robinson, J., Ramanarayanan, P., Sattiraju, S., Schroeder, T., Williams, S. & Yashar, P. (2008). Low-k interconnect stack with thick metal 9 redistribution layer and Cu die bump for 45nm high volume manufacturing. In *Proceedings of the IEEE International Interconnect Technology Conference*, pp. 216–218. Burlingame, CA: IEEE Electron Devices Society.

Jarausch, K., Thomas, P., Leonard, D.N., Twesten, R. & Booth, C.R. (2009). Four-dimensional STEM-EELS: Enabling nanoscale chemical tomography. *Ultramicroscopy* **109**, 326–337.

Kawase, N., Kato, M., Nishioka, H. & Jinnai, H. (2007). Transmission electron microtomography without the "missing wedge" for quantitative structural analysis. *Ultramicroscopy* **107**, 8–15.

Ke, X., Bals, S., Romo-Negreira, A., Hantschel, T., Bender, H. & Van Tendeloo, G. (2009). TEM sample preparation by FIB for carbon nanotube interconnects. *Ultramicroscopy* **109**, 1353–1359.

Kolb, U., Gorelik, T., Kübel, C., Otten, M.T. & Hubert, D. (2007). Towards automated diffraction tomography: Part I—Data acquisition. *Ultramicroscopy* **107**, 507–513.

Kreupl, F., Graham, A.P., Duesberg, G.S., Steinhögl, W., Liebau, M., Unger, E. & Hönlein, W. (2002). Carbon nanotubes in interconnect applications. *Microelectron Eng* **64**, 399–408.

Li, H., Srivastava, N., Mao, J.F., Yin, W.Y. & Banerjee, K. (2007). Carbon nanotube vias: A reality check. In *2007 IEEE International Electron Devices Meeting—IEDM '07*, pp. 207–210. Washington, DC: IEEE Electron Devices Society.

Li, J., Ye, Q., Cassell, A., Ng, H.T., Stevens, R., Han, J. & Meyyappan, M. (2003). Bottom-up approach for carbon nanotube interconnects. *Appl Phys Lett* **82**, 2491–2493.

Midgley, P.A. & Weyland, M. (2003). 3D electron microscopy in the physical sciences: The development of Z-contrast and EFTEM tomography. *Ultramicroscopy* **96**, 413–431.

Möbus, G., Doole, R.C. & Inkson, B.J. (2003). Spectroscopic electron tomography. *Ultramicroscopy* **96**, 433–451.

Möbus, G. & Inkson, B.J. (2001). Three-dimensional reconstruction of buried nanoparticles by element-sensitive tomography based on inelastically scattered electrons. *Appl Phys Lett* **79**, 1369–1371.

Montoya, E. (2007). Focused ion beam: A way to prepare high quality TEM specimens. Ph.D. thesis, University of Antwerp.

Montoya, E., Bals, S., Rossell, M.D., Schryvers, D. & Van Tendeloo, G. (2007). Evaluation of top, angle, and side cleaned FIB samples for TEM analysis. *Microsc Res Techniq* **70**, 1060–1071.

Nihei, M., Kawabata, A. & Awano, Y. (2003). Direct diameter-controlled growth of multiwall carbon nanotubes on nickel-silicide layer. *Jpn J Apply Phys* **42**, L721–L723.

Nihei, M., Kondo, D., Kawabata, A., Sato, S., Shioya, H., Sakaue, M., Iwai, T., Ohfuti, M. & Awano, Y. (2005). Low-resistance multi-walled carbon nanotube vias with parallel channel conduction of inner shells. In *Proceedings of the IEEE 2005 International Interconnect Technology Conference*, pp. 234–236. Burlingame, CA: IEEE Electron Devices Society.

Romo-Negreira, A., Cott, D.J., Verhulst, A.S., Esconjauregui, S., Chiodarelli, N., Ek-Weis, J., Whelan, C.M., Groeseneken, G., Heyns, M.M., De Gendt, S. & Vereecken, P.M. (2008). Growth and integration of high-density CNT for BEOL interconnects. In *Materials Research Society Symposium Proceedings*, p. 1079-N06-01. San Francisco, CA: Materials Research Soiety.

Romo-Negreira, A., Richard, O., De Gendt, S., Maex, K., Heyns, M.M. & Vereecken, P.M. (2009). Selective growth of carbon nanotubes on silicon from electrodeposited nickel catalyst. *Sci Adv Mater* **1**, 86–92.

Sato, S., Nihei, M., Mimura, A., Kawabata, A., Kondo, D., Shioya, H., Taisuke, W., Mishima, M., Ohfuti, M. & Awano, Y. (2006). Novel approach to fabricating carbon nanotube via interconnects using size-controlled catalyst nanoparticles. In *Proceedings of the IEEE 2006 International Interconnect Technology Conference*, pp. 230–232. Burlingame, CA: IEEE Electron Devices Society.

Srivastava, N., Joshi, R.V. & Banerjee, K. (2005). Carbon nanotube interconnects: Implications for performance, power dissipation and thermal management. In *IEEE International Electron Devices Meeting (IEDM) 2005, Technical Digest*, pp. 257–260. Washington, DC: IEEE Electron Devices Society.

Steinlesberger, G., Engelhardt, M., Schindler, G., Steinhögl, W., Von Glasow, A., Mosig, K. & Bertagnolli, E. (2002). Electrical assessment of copper damascene interconnects down to sub-50 nm feature sizes. *Microelectron Eng* **64**, 409–416.

Thompson, K., Lawrence, D., Larson, D.J., Olson, J.D., Kelly, T.F. & Gornam, B. (2007). *In situ* site-specific specimen preparation for atom probe tomography. *Ultramicroscopy* **107**, 131–139.

Turner, S., Tavernier, S.M.F., Huyberechts, G., Biermans, E., Bals, S., Batenburg, K.J. & Van Tendeloo, G. (2009). Assisted spray pyrolysis production and characterisation of ZnO nanoparticles with narrow size distribution. *J Nanopart Res*; doi10.1007/s11051-009-9630-1. Available at http://www.springerlink.com/content/9125366866701j2m/.

Yaguchi, T., Konno, M., Kamino, T. & Watanabe, M. (2008). Observation of three-dimensional elemental distributions of a Si device using a 360 degrees-tilt FIB and the cold field-emission STEM system. *Ultramicroscopy* **108**, 1603–1615.

Zhang, C., Cott, D., Chiodarelli, N., Vereecken, P., Robertson, J. & Whelan, C.M. (2008). Growth of carbon nanotubes as horizontal interconnects. *Phys Sta Sol (b)* **245**, 2308.